Improved Diffraction Computation with a Hybrid C-RCWA-Method

Joerg Bischoff, Timbre Technologies, INC. A TEL Company, 2953 Bunker Hill Lane #301, Santa Clara, California 95054, USA and Tokyo Electron Germany/ Moritzburger Weg 67d, D-01109 Dresden, Germany. Email: jbischoff@timbrecom.com

ABSTRACT

The Rigorous Coupled Wave Approach (RCWA) is acknowledged as a well established diffraction simulation method in electro-magnetic computing. Its two most essential applications in the semiconductor industry are in optical scatterometry and optical lithography simulation. In scatterometry, it is the standard technique to simulate spectra or diffraction responses for gratings to be characterized. In optical lithography simulation, it is an effective alternative to supplement or even to replace the FDTD for the calculation of light diffraction from thick masks as well as from wafer topographies. Unfortunately, the RCWA shows some serious disadvantages particularly for the modelling of grating profiles with shallow slopes and multilayer stacks with many layers such as extreme UV masks with large number of quarter wave layers. Here, the slicing may become a nightmare and also the computation costs may increase dramatically. Moreover, the accuracy is suffering due to the inadequate staircase approximation of the slicing in conjunction with the boundary conditions in TM polarization. On the other hand, the Chandezon Method (C-Method) solves all these problems in a very elegant way, however, it fails for binary patterns or gratings with very steep profiles where the RCWA works excellent. Therefore, we suggest a combination of both methods as plug-ins in the same scattering matrix coupling frame. The improved performance and the advantages of this hybrid C-RCWA-Method over the individual methods is shown with some relevant examples.

Keywords: Optical Scatterometry, Lithography Simulation, Grating Diffraction

1. Introduction

Over the last couples of years, the RCWA [1,2] has matured and become one of the most popular method for grating diffraction simulation. Although the RCWA is very universal and in general very robust it has also some essential disadvantages. Those arise mainly from the necessity of slicing which is an inevitable component of the RCWA. Here, it may well be that a large number of slices is required to ensure convergence particularly for shallow slopes and high contrast materials. Even worse, the method fails in extreme TM polarization cases [3] because the boundary conditions in a slice do not reflect the real boundary conditions of the slope. Usually, the number of slices also depends on the sidewall angle of the grating profile, i.e. the steeper the angle the less slices are required. And in the case of a binary grating with perpendicular slopes the slicing becomes obsolete.

A quite interesting alternative is the coordinate transformation method introduced and extended by Chandezon and Granet [4]. The C-method does not require any slicing because it transforms the profile into a flat layer in the new curvilinear coordinate system. Here, the problem is a sort of opposite compared to the RCWA. The method begins to fail for very steep profiles due to the decreasing sampling density of the profile around the steep slopes. An appropriate remedy to overcome this issue is to introduce an additional coordinate transformation for the horizontal axes a.k.a. adaptive resolution method [5] though this does not enable mean that exact 90 degrees slopes can be treated. Another restriction of the C-method is that it cannot handle overhanging profiles in its natural form.

In summary, both methods show advantages and disadvantages which are supplementary. Therefore, the strengths of both methods can be combined when they are weaved into the same S-matrix frame algorithm. In doing so, the idea is to chop a multilayer grating into parts and treat each part with the more appropriate diffraction method, i.e. either RCWA or C-method. Eventually, all the chunks are coupled together based on S-matrix methods. As usual, this shall be preferably done in a bottom-up fashion. Before coming to the details of how to link the C-method solutions with those of the RCWA in section 3, a short review of both methods shall be given in the next section. This is followed by some numerical results given in section 4 showing the superiority of the hybrid approach compared to the individual methods.

2. Review of the C-method and the RCWA

The Coordinate Transformation Method (C-Method) a.k.a. Chandezon Method was introduced in 1980 by Jean Chandezon's famous paper [4]. The main idea behind this method is to express Maxwell's Equation in general curvilinear coordinates (given below in Einstein's sum notation):

$$\begin{aligned} \xi^{ijk}\,\partial_j E_k &= -ik\sqrt{g}\cdot g^{ij}\cdot Z\cdot H_j \\ \xi^{ijk}\,\partial_j Z H_k &= ik\varepsilon\sqrt{g}\cdot g^{ij}\cdot E_j \end{aligned} \tag{1}$$

Here, nonmagnetic materials are assumed with $\mu = 1$ and Z is the so called free space impedance with:

$$Z = \sqrt{\mu_0/\varepsilon_0}$$

ξ is the Levi-Civita indicator which is defined as:

$$\begin{aligned} \xi^{ijk} &= +1, if\ (ijk)\ is\ an\ even\ permutation\ of\ (123) \\ \xi^{ijk} &= -1, if\ (ijk)\ is\ an\ odd\ permutation\ of\ (123) \\ \xi^{ijk} &= 0, otherwise \end{aligned}$$

Moreover, g^{ij} is the metric tensor of the coordinate transformation and g is its determinant. This metric tensor is defined by means of the partial derivatives of the new coordinates $\bar{x}$ for the Cartesian coordinates x ($x_1 = x$, $x_2 = y$, $x_3 = z$):

$$g^{ij} = \sum_{n=1}^{3} \bar{a}_n^i \cdot \bar{a}_n^j \ \text{ and } \ \bar{a}_j^i = \frac{\partial \bar{x}^i}{\partial x_j} \tag{2}$$

In the case of a line/space grating with the period p and a profile function y = a(x), the coordinate transformation may be expressed by (see fig. 1for the coordinate directions):

$$\begin{aligned} \bar{x}^1 &= x \\ \bar{x}^2 &= y - a(x) \\ \bar{x}^3 &= z \end{aligned} \tag{3}$$

Then, the computation of the partial derivatives results in:

$$\begin{array}{lll} \frac{\partial \bar{x}^1}{\partial x} = 1 & \frac{\partial \bar{x}^2}{\partial x} = -\dot{a} & \frac{\partial \bar{x}^3}{\partial x} = 0 \\ \frac{\partial \bar{x}^1}{\partial y} = 0 & \frac{\partial \bar{x}^2}{\partial y} = 1 & \frac{\partial \bar{x}^3}{\partial y} = 0 \\ \frac{\partial \bar{x}^1}{\partial z} = 0 & \frac{\partial \bar{x}^2}{\partial z} = 0 & \frac{\partial \bar{x}^3}{\partial z} = 1 \end{array} \tag{4}$$

And the metric tensor is:

$$g^{ij} = \begin{pmatrix} 1 & -\dot{a} & 0 \\ -\dot{a} & 1 + \dot{a}\cdot\dot{a} & 0 \\ 0 & 0 & 1 \end{pmatrix} \tag{5}$$

The determinant is g = 1 as can be verified easily. A metric tensor for a crossed grating can be derived straightforwardly in an analogous manner.

Like the RCWA, the C-method is a modal method, i.e. the Maxwell equations are Fourier transformed. Because of the periodicity character of the grating, the derivatives in the grating plane can be written as:

$\partial_1 \rightarrow i\beta\ \beta = \sin\theta_i + m\frac{\lambda}{p}$ (m = diffraction order, λ = wavelength, θ_i = angle of incidence, p = grating period) for the 1D non-conical grating case.

Furthermore, in this case the azimuthal angle φ is equal to 0 and consequently, the polarization cases TE and TM decouple. Then, half of the components of the electromagnetic field disappear in either polarization case, i.e. $E_1 = E_2 = H_3 = 0$ for TE-polarization and $H_1 = H_2 = E_3 = 0$ for TM-polarization. Eliminating the normal components, H_2 in TE or E_2 in TE, and applying the correct Fourier factorization rules, eventually results in the following first order differential equation systems:

$$\text{TE: } \partial_2 \begin{pmatrix} E_3 \\ ZH_1 \end{pmatrix} = \begin{pmatrix} d\cdot\beta & -c \\ \beta\cdot c\cdot\beta - (\varepsilon) & \beta\cdot d \end{pmatrix}\cdot\begin{pmatrix} E_3 \\ ZH_1 \end{pmatrix} \quad \text{TM: } \partial_2 \begin{pmatrix} ZH_3 \\ E_1 \end{pmatrix} = \begin{pmatrix} d\cdot\beta & \left(\frac{1}{\varepsilon}\right)^{-1}\cdot c \\ 1-\beta\cdot(\varepsilon)^{-1}\cdot c\cdot\beta & \beta\cdot d \end{pmatrix}\cdot\begin{pmatrix} ZH_3 \\ E_1 \end{pmatrix} \quad (6)$$

The abbreviations c and d are: $c = (1+\dot{a}\cdot\dot{a})^{-1}$, $d = c\cdot\dot{a}$ and $\dot{a} = \frac{\partial a}{\partial x}$ is the derivative of the grating profile function .

There is some beauty in these equations, which should be pointed out briefly. First of all, they include the regular RCWA case. This can be verified by inserting a flat interface with $\dot{a} = 0$. Because of d = 0, the diagonal sub-matrices of both DES disappear and (6) can be transformed in the familiar second order DES of the RCWA (here the TE polarization case is exemplified), i.e.:

$$\frac{\partial^2}{\partial {x_2}^2} E_3 = \partial_{22} E_3 = \left({\beta_1}^2 - (\varepsilon)\right)\cdot E_3 = D_e\cdot E_3 \quad (7)$$

The solution of the RCWA follows the well established lines. First, the second order DES is transformed into an Eigen equation. Then, the Eigen equation is solved. Formally, this can be written as:

$$D_e = W_e\cdot\ \lambda^2\cdot {W_e}^{-1} \quad (8)$$

Here, the term W_e represents the matrix of the Eigen vectors and λ^2 is a diagonal matrix with the Eigen values. By setting:

$$\begin{pmatrix} v^- \\ v^+ \end{pmatrix} = {W_e}^{-1}\cdot\begin{pmatrix} E_3 \\ ZH_1 \end{pmatrix} \quad (9)$$

a differential equation system with decoupled individual modes is obtained:

$$\partial_{22}\begin{pmatrix} v^- \\ v^+ \end{pmatrix} = \lambda^2\cdot\begin{pmatrix} v^- \\ v^+ \end{pmatrix} \quad (10)$$

It can be solved straightforwardly for the individual modes. Thus, the propagation of the individual modes in a RCWA slice with the height h can be expressed as:

$$\begin{pmatrix} v^- \\ v^+ \end{pmatrix} = \begin{pmatrix} e^{-i\lambda h} & 0 \\ 0 & e^{+i\lambda h} \end{pmatrix}\cdot\begin{pmatrix} v^- \\ v^+ \end{pmatrix} \quad (11)$$

The TM polarization case can be treated in a similar manner.

On the other hand, the assumption can be made that the warped layer is a thin film rather than being only piecewise homogeneous. Then, the matrix ε becomes a scalar and the two DES's of first order in (6) can be reduced to DES's which exhibit the same Eigen systems (!), namely:

$$\partial_2\begin{pmatrix} F \\ G \end{pmatrix} = \begin{pmatrix} d\cdot\beta & -c \\ \beta\cdot c\cdot\beta - \varepsilon & \beta\cdot d \end{pmatrix}\cdot\begin{pmatrix} F \\ G \end{pmatrix} \quad (12)$$

where $F = E_3$ and $G = ZH_1$ for TE polarization and $F = -ZH_3/\varepsilon$ and $G = E_1$.for TM-polarization, respectively. Again, the differential equation system can be transformed in an Eigen equation. Its Eigen decomposition can be written as:

$$M^{(p,q)}\begin{pmatrix} {F_m}^{(p,q)} \\ {G_m}^{(p,q)} \end{pmatrix} = \lambda^{(p,q)}\begin{pmatrix} {F_m}^{(p,q)} \\ {G_m}^{(p,q)} \end{pmatrix} \tag{13}$$

Here, ${F_m}^{(p,q)}$ and ${G_m}^{(p,q)}$ are the Eigenvectors and $\lambda^{(p,q)}$ is the Eigen value. In order to couple the fields, we need to write down the sums of all up- and down waves:

$$\begin{aligned} {F_\pm}^{(p,q)} &= \sum_{m,n} e^{i\beta_m x^1} {F_{m,n}}^{(p,q)\pm} e^{i{\lambda_n}^{(p,q)\pm} x^3} \cdot {\nu_n}^{(p,q)\pm} \\ {G_\pm}^{(p,q)} &= \sum_{m,n} e^{i\beta_m x^1} {G_{m,n}}^{(p,q)\pm} e^{i{\lambda_n}^{(p,q)\pm} x^3} \cdot {\nu_n}^{(p,q)\pm} \end{aligned} \tag{14}$$

Furthermore, p and q are the medium index and the interface index, ${F_{m,n}}^{(p,q)\pm}$ and ${F_{m,n}}^{(p,q)\pm}$ are the Eigen vector elements of the order (m,n), ${\lambda_n}^{(p,q)\pm}$ is the Eigen value of order n and ${\nu_n}^{(p,q)\pm}$ are the unknown amplitudes of the Eigen modes. For the propagation through an interface q between two materials, one has to solve the Eigen problem for both materials ε_p and ε_{p+1} followed by the application of the boundary conditions, i.e. ${F_\pm}^{(p,q)} = {F_\pm}^{(p+1,q)}$ and ${G_\pm}^{(p,q)} = {G_\pm}^{(p+1,q)}$. Sorted for up- and down- waves, this procedure results in the following short-hand matrix equation:

$$\begin{pmatrix} F^{(p+1,q)+} & F^{(p+1,q)-} \\ G^{(p+1,q)+} & G^{(p+1,q)-} \end{pmatrix} \cdot \begin{pmatrix} \nu^{(p+1,q)+} \\ \nu^{(p+1,q)-} \end{pmatrix} = \begin{pmatrix} F^{(p,q)+} & F^{(p,q)-} \\ G^{(p,q)+} & G^{(p,q)-} \end{pmatrix} \cdot \begin{pmatrix} \nu^{(p,q)+} \\ \nu^{(p,q)-} \end{pmatrix} \tag{15}$$

Due to the S-matrix coupling schema, it can be sorted for the cause- and response waves resulting in:

$$\begin{pmatrix} \nu^{(p+1,q)+} \\ \nu^{(p,q)-} \end{pmatrix} = \begin{pmatrix} F^{(p+1,q)+} & -F^{(p,q)-} \\ G^{(p+1,q)+} & -G^{(p,q)-} \end{pmatrix}^{-1} \cdot \begin{pmatrix} -F^{(p+1,q)-} & F^{(p,q)+} \\ -G^{(p+1,q)-} & G^{(p,q)+} \end{pmatrix} \cdot \begin{pmatrix} \nu^{(p+1,q)-} \\ \nu^{(p,q)+} \end{pmatrix} \tag{16}$$

Next, the propagation from one interface to the next interface shall be considered. Basically there are two cases, either the next interface has the same derivative of the profile function, i.e. $\dot{a}_{q+1}(x) = \dot{a}_q(x)$ or it is different which also means that there are different coordinate systems. In the first case, the solution is trivial. It corresponds to the propagation in a thin film or to the propagation of the Bragg modes in a RCWA slice and thus resembles formula (11). The second case is more difficult and the general approach is to describe the fields at one coordinate system by means of the coordinates of the adjacent (below or above) interface. Regarding the coupling of the fields, two methods are suggested – the half spectrum coupling [6] and the hybrid spectrum coupling [7]. The formula for the half spectrum propagation from interface q to interface q+1 is given below.

$$\begin{pmatrix} \nu^{(p,q)+} \\ \nu^{(p,q-1)-} \end{pmatrix} = \begin{pmatrix} 0 & \left(F^{(p,q)+}\right)^{-1} \cdot \tilde{F}^{(p,q-1)+} \\ \left(F^{(p,q-1)-}\right)^{-1} \cdot \tilde{F}^{(p,q)-} & 0 \end{pmatrix} \cdot \begin{pmatrix} \nu^{(p,q)-} \\ \nu^{(p,q-1)+} \end{pmatrix} \tag{17}$$

The computation recipe for the ~ term is given by:

$${\tilde{F}_{m,n}}^{(p,q)\pm} = \sum_l {L_{m-l,n}}^{(p,q)\pm} \cdot {F_{l,n}}^{(p,q)\pm} \text{ and } {L_{m,n}}^{(p,q)\pm} = \frac{1}{p}\int_0^d e^{i{\lambda_n}^{(p,q)\pm} \cdot [a_{q-1}(x) - a_q(x)]} \cdot e^{-im\frac{2\pi x}{p}} dx \tag{18}$$

More details can be found in [6] and [7].

After having provided these ingredients, the assembling of the S-matrix of the whole stack follows mainly the coupling rules in [8].

3. Combination of the Methods

In summary of section 2, the RCWA method slices a given interface and then propagates the electromagnetic fields from slice to slice whereas the C-method directly solves the propagation of the electromagnetic field through an interface by means of formulating and solving the Maxwell equations in a curvilinear coordinate system. Moreover, it was discussed that more than one coordinate transformation is required when there are more than one interface that are not parallel to each other.

Now, the key of the combination of the two methods consists in the idea to propagate the electromagnetic fields from a curved interface q-1 where the C-method is be applied to a plain interface q that is a boundary of a RCWA slice and vice versa. The scenario of a RCWA slice embedded between curved interfaces is depicted in figure 1.

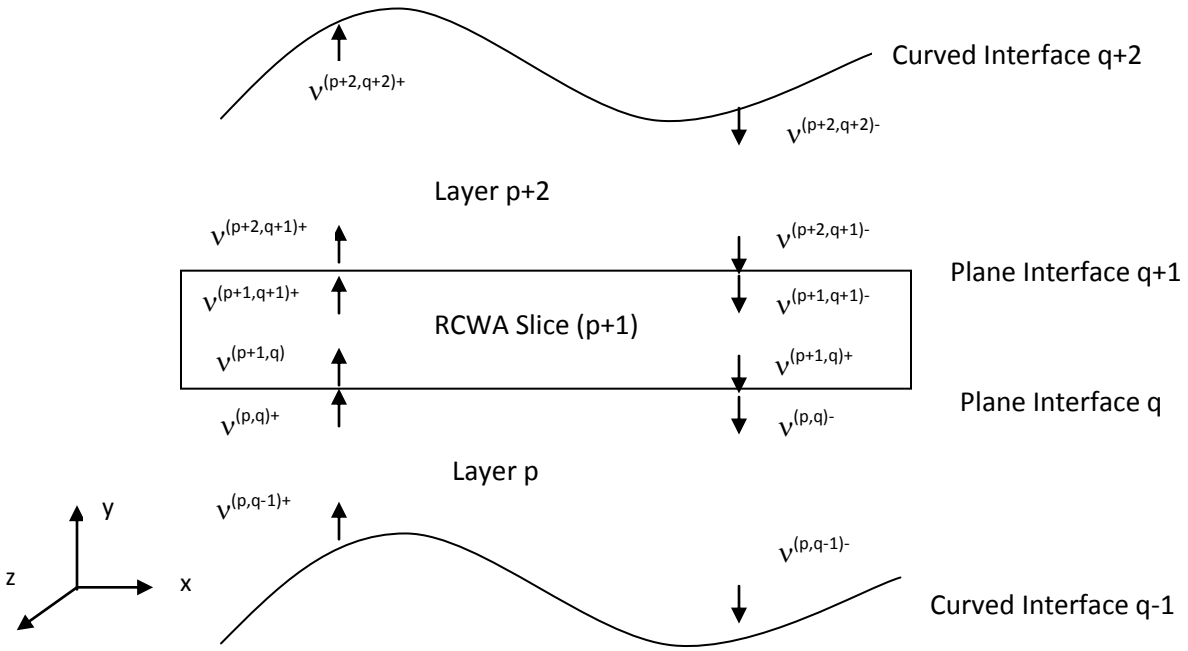

Figure 1: Layer Schema for hybrid C-RCWA

A flat interface forming one boundary of a RCWA slice is a special case of a curved interface and it is naturally not parallel to any other curved interface. Therefore, the propagation from a curved interface to a flat interface and vice versa has to be based on either the half- or hybrid spectrum coupling method mentioned in the previous section. However, the treatment can be simplified a bit due to the special form of the flat interface since it does not require to solve an Eigen problem but it can utilize the Rayleigh modes directly. Moreover, the matrix of the Eigen vectors becomes a unit matrix and the interface function becomes a constant. Consequently, the propagation from the curved interface q-1 to the plain interface q through layer p (17) can be simplified correspondingly.

As a next step, the fields need to be propagated into the RCWA slice. Generally, the formulation for the C-method as well as for the RCWA is based on a direct propagation step through the interface (compare for example equation (16) of this paper and formulas 5-7 in [8]). In order to connect both methods, the junction has to be put directly on the flat interface bordering the RCWA slice. This issue can be overcome by applying the following procedure. First, switch from the up and down modes to the Fourier modes of the transversal fields, e.g. E_3 and ZH_1 for TE-polarisation in one of the methods (e.g. C-method). Secondly, cross the interface boundary by applying the boundary conditions of the

electromagnetic field. Then, continue by switching back from the Fourier modes of the transversal fields while tacitly changing the method (i.e. continue with RCWA slice propagation).

This whole procedure shall be exemplified with the layer stack in figure 1. Let's assume we are arrived behind the curved interface q-1 by applying the C-method. Then, the first step consists in propagating the up and down modes from interface q-1 to the lower boundary of the RCWA slice (interface q). This can be done by either applying the half- or the hybrid spectrum method referred to in section 2 of this paper. When the half spectrum method is applied, equation (17) can be utilized directly while taking advantage of the matter of fact that interface q is flat. Next, the modes are switched to E_3 and ZH_1 using formula (15) followed by crossing the interface through the assumption of continuity of the transversal modes (a.k.a. boundary conditions). While performing this step, the border from C-method to RCWA is crossed and the further processing is based on RCWA formulas. This means, the modes are switched back to up and down modes by using formula (9) and then propagated from the bottom to the top (lower side of interface q+1) of the RCWA slice by using expression (11). Of course, it is recommended to do all the propagation and coupling in the most computation efficient way as detailed for instance in reference [8]. The further propagation from the lower side of interface q+1 to the curved interface q+2 has to be carried out in an opposite way.

4. Modeling

The first modelling example is shown in figure 2. Here, the intention is to demonstrate the superiority of the C-method and to show how bad the RCWA converges for high contrast material with a shallow profile slope. The grating is a trapezoid with a pitch of 1 micron, a duty ratio of 1:1 and 45 degrees side wall angle made from aluminium. The light with 633 nm wavelength is incident from normal direction.

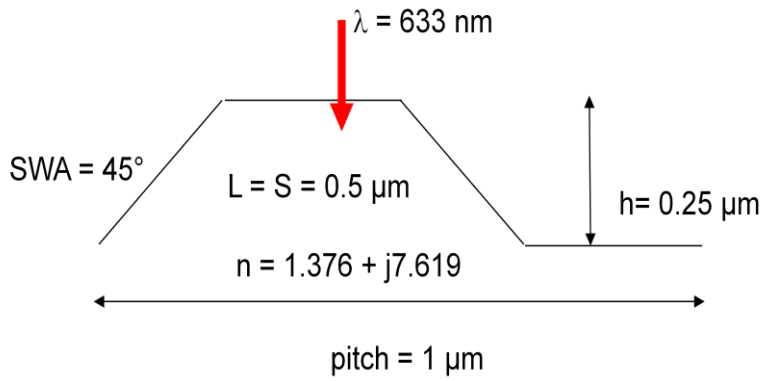

Figure 2: Modeling example 1 - Aluminum trapezoid

The order convergence for TE and TM is shown in figure 3. The RCWA was run with 5, 10, 25 and 50 slices. It can be seen that the convergence is quite different for the two polarization cases. Apparently, the RCWA converges to the same results as the C-method for TE when the number of slices is sufficient large. Nevertheless, the convergence is still considerably slower compared to the C-method. While the C-method requires only as few as about ±8 orders to converge, the RCWA requires at least ±20 to 25 orders.

The situation becomes much worse for TM polarization. Here, a decent convergence for the TM case cannot be seen at all, no matter how many slices are utilized. On the other hand, the C-method results agree well with the results obtained from the IESMP[9] which serves as a reference (41.73% reflectivity in TM and 6.93% in TE for the 0. order).

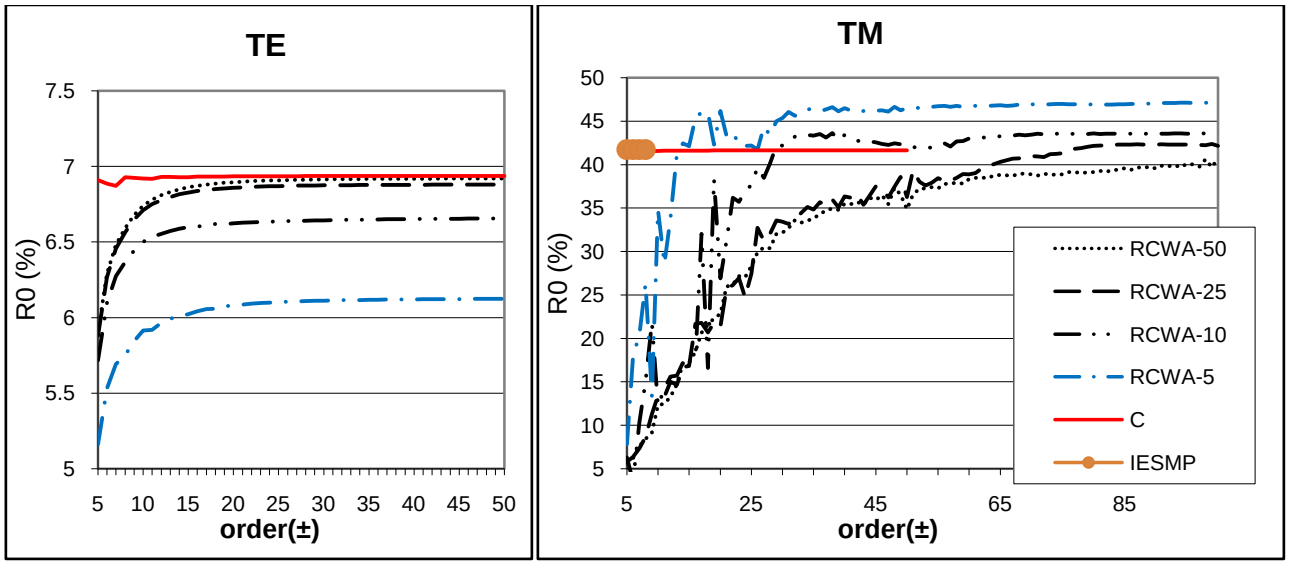

Figure 3: Comparison of simulated diffraction efficiencies of the 0. order in reflection vs. truncation order for example 1 - aluminum trapezoid (see fig. 2) computed by RCWA and C-method (LHS: TE polarization, RHS: TM polarization). The IESMP result serves as a reference.

In the second example, the C-RCWA simulations are compared with a pure RCWA simulation with the example of a binary grating made of Silicon covered with a dielectric layer (e.g., photoresist). The grating setup is depicted in figure 4.

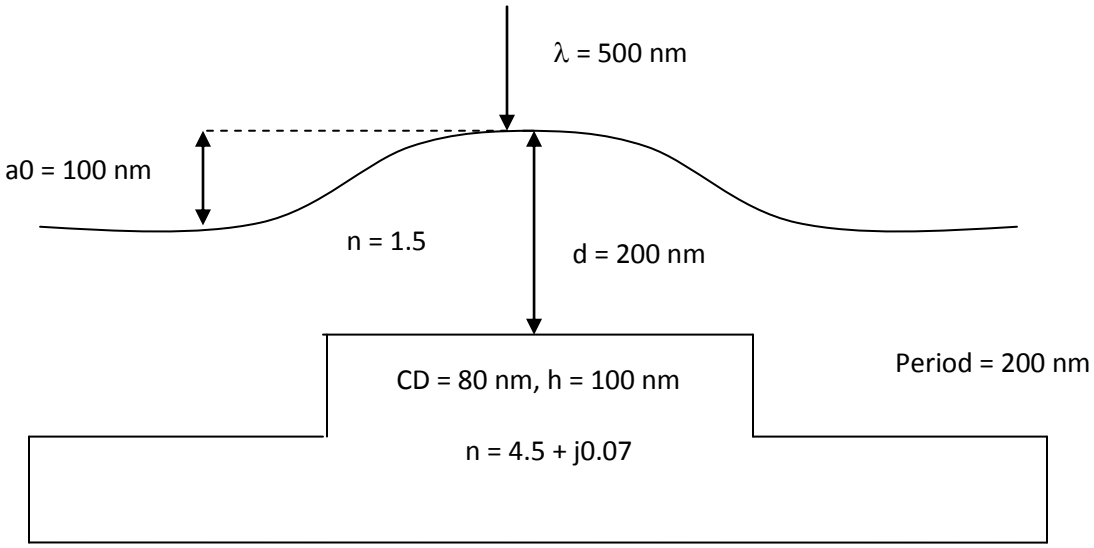

Figure 4: Modeling example 2 – Binary Silicon grating covered with a dielectric layer

The zero order diffraction efficiencies in reflection (measured in %) for the second example are shown in figure 5. It can be concluded that the RCWA requires many slices to come close to the C-RCWA results.

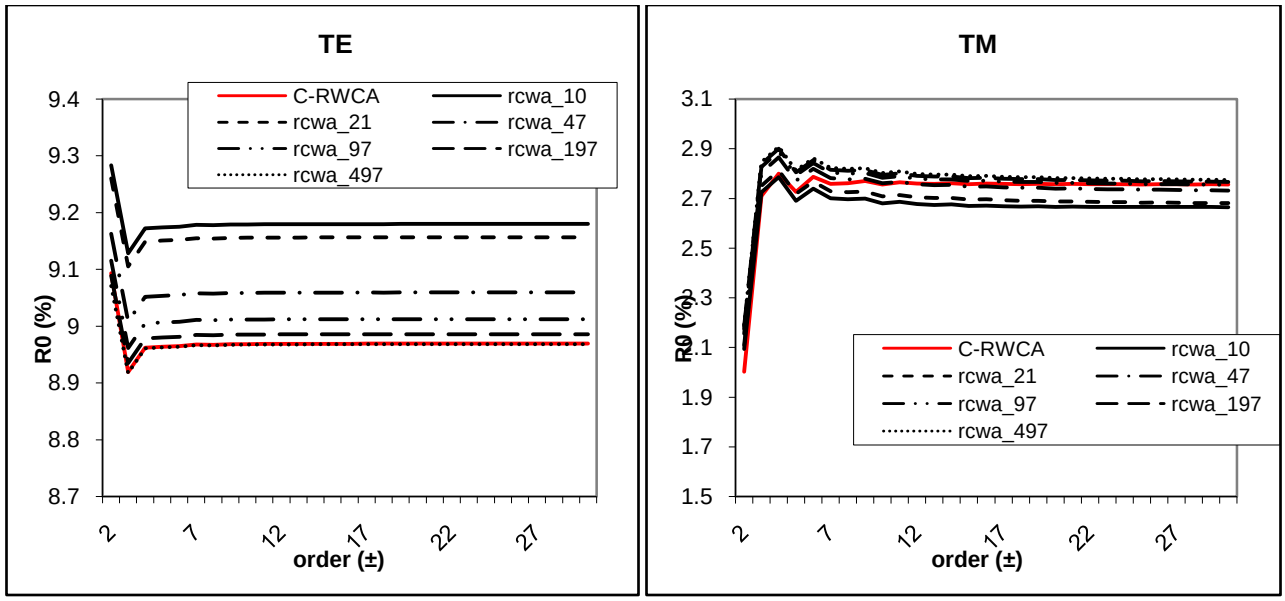

Figure 5: Diffraction efficiencies of the 0. order in reflection vs. truncation order for example 2 – Binary Silicon grating coated with a dielectric (see fig. 4). The C-RCWA is compared with RCWA computations with different slice number (i.e. 10, 21, 47, 97, 197 and 497).

Another way to present these results is to plot the reflectance versus the number of slices (slice convergence) which is shown in figure 6. The diamonds show the RCWA result for converged order (i.e. ±30 orders. It should be stated here that the slicing for the sinusoidal was done in a way to keep the CD change from slice to slice constant rather than just chosing slices of equal thickness to ensure the best possible accuracy with minimum slice number. A Finite Element Method based solver[10] serves as a reference (triangles). The FEM results are plotted versus the degrees of freedom (DOF). It is quite obvious that the hybrid C-RCWA results (pink squares) and the FEM results converge to the same values both in TE and TM polarization. The C-RCWA results are shown as a straight line since they neither depend on a slice number nor on degrees of freedom.

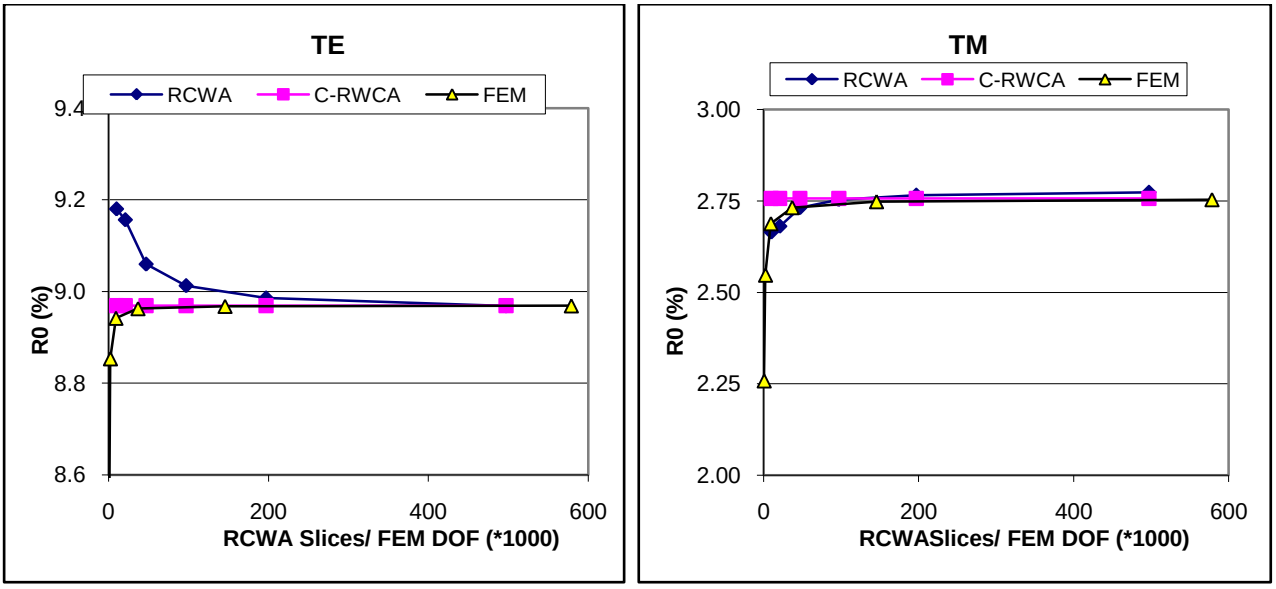

Figure 6: Diffraction efficiencies of the 0. order in reflection vs. slice number for RCWA/ degrees of freedom (DOF) for FEM method for example 2 – Binary Silicon grating covered with a dielectric (see fig. 4), truncation order = ±30 for RCWA and C-RCWA.

Please note that the hybrid C-RCWA needs only three Eigensolutions: two for either side of the curved interface and one for the buried binary grating. In contrast, the pure RCWA requires at least about 400 -500 slices in TE to come close which translates into the same number of Eigen solutions. Moreover, the pure RCWA TM result does not even quite converge at 500 slices. This outcome is quite a bit surprising because the sliced sinusoidal layer is purely dielectric and the author is not aware that issues have been reported in the literature related to the RCWA modeling of dielectric layers.

Our third example discusses defect issues in EUV lithography. The EUV mask consists of large number of high and low index, quarter wave double layers. Fourty double layers are required to ensure a suffcient reflectivityof about 70% due to the low difference in n of the available materials such as molybdenum and silicon (MoSi) for EUV radiation.

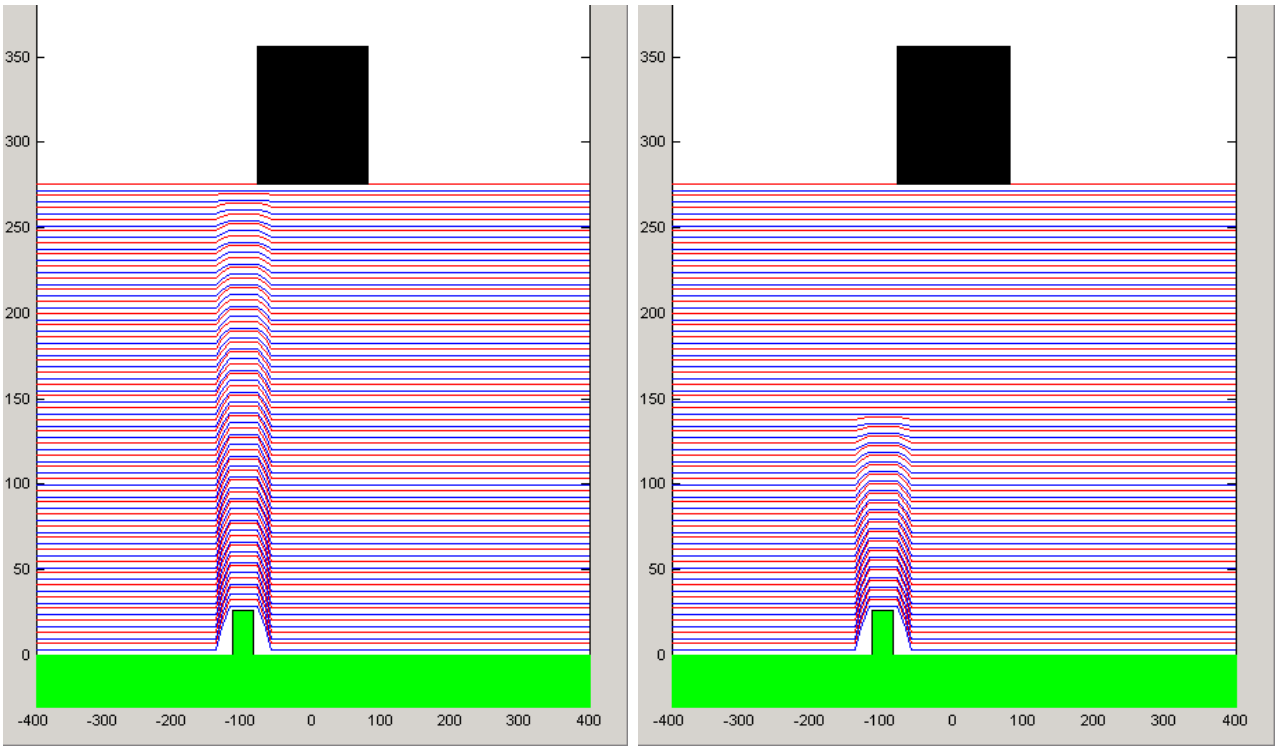

Figure 7: Cross section of a EUV multilayer mask with a binary substrate defect that causes a gradually attenuated deformation of the multilayer system from bottom to top. The defect is lateral offset relative to the absorber line (LHS: all layers are deformed, RHS: only the lower 40 layers are deformed whereas the upper 40 layers are planarized).

As discussed in [11], the lithographic imaging modeling of EUV may become very cumbersome and costly when the impact of mask defects shall be investigated. Actually, this means that the MoSi layers cannot be treated as thin film anymore but need to be modeled as diffractive layers instead. Consequently, a huge number of discretization points is required in FDTD to model all subtleties of the deformed multilayer stack adequately. Similarly, one would need many slices in RCWA and the slicing itself may quickly cause some headache not to talk about accuracy issues as observed in the previous example.

Here, our C-RCWA method may greatly help to reduce the computational efforts since it is adapted to the problem in a very natural way. While the multilayer can be modeled with the C-method, the binary defect and the binary absorber are treated with the RCWA. Figure 7 depicts the layer stack with a defect in the substrate which is laterally offset relative to an absorber line on top of the stack. The left hand side shows the case where all layers are deformed whereas the top half of the multilayers are planarized in the right hand side of the figure. Lithographers are very interested to predict the impact of the defect on the aerial image and eventually on the CD.

Our aerial image simulation follows the established models of partial coherent imaging (compare fig. 2 in [11]) with the mask diffraction computed by means of the C-RCWA. The simulations are based on the following settings:

Optical system: NA = 0.45, σ = 0.3, λ = 13.4 nm, reduction ratio = 4.

EUV mask: multilayer: 40 double layers of Si/ Mo (thickness = 4 nm/ 2.9 nm, n_{Si} = 0.999931-j0.00182109, n_{Mo} = 0.922737-j0.0062202), Si substrate, Si defect: height = 26 nm, width = 30 nm, Cr absorber: CD = 160 nm, height = 80 nm, $n_{Absorber}$ = 0.933328-j0.0381982. (all CD's are measured on the mask level).

First, we have investigated the impact of the lateral offset of the defect relative to the center of the absorber line on the aerial image. To this end the defect was moved in steps of 20 nm from the center of the absorber line to the left, resulting in relative positions of x0 = 0, 20, 40, 60, 80 and 100 nm (measured in mask coordinates). The resulting aerial image curves are plotted in figure 8. Additionally, the defect free case is shown as a reference. Apparently, the aerial image is centered when there is no offset x0 = 0 (red solid line) and almost coincides with the defect free case (black solid line). The nominal CD of the aerial image on the wafer level is approximately 40 nm as anticipated. When moving the defect to the left by only 20 or 40 nm, almost no difference in the aerial image can be seen. Obviously, the defect is still well hidden under the absorber and cannot cause much trouble. However, a further increase of the offset causes a considerable shift of the left slope of the aerial image to the left while the right slope remains in the same location as for x0 = 0 resulting in an increase of the CD by almost 20 nm for x0 = 100 nm. Now, it can be clearly seen that the interferences in the multilayer may have a strong impact on the imaging.

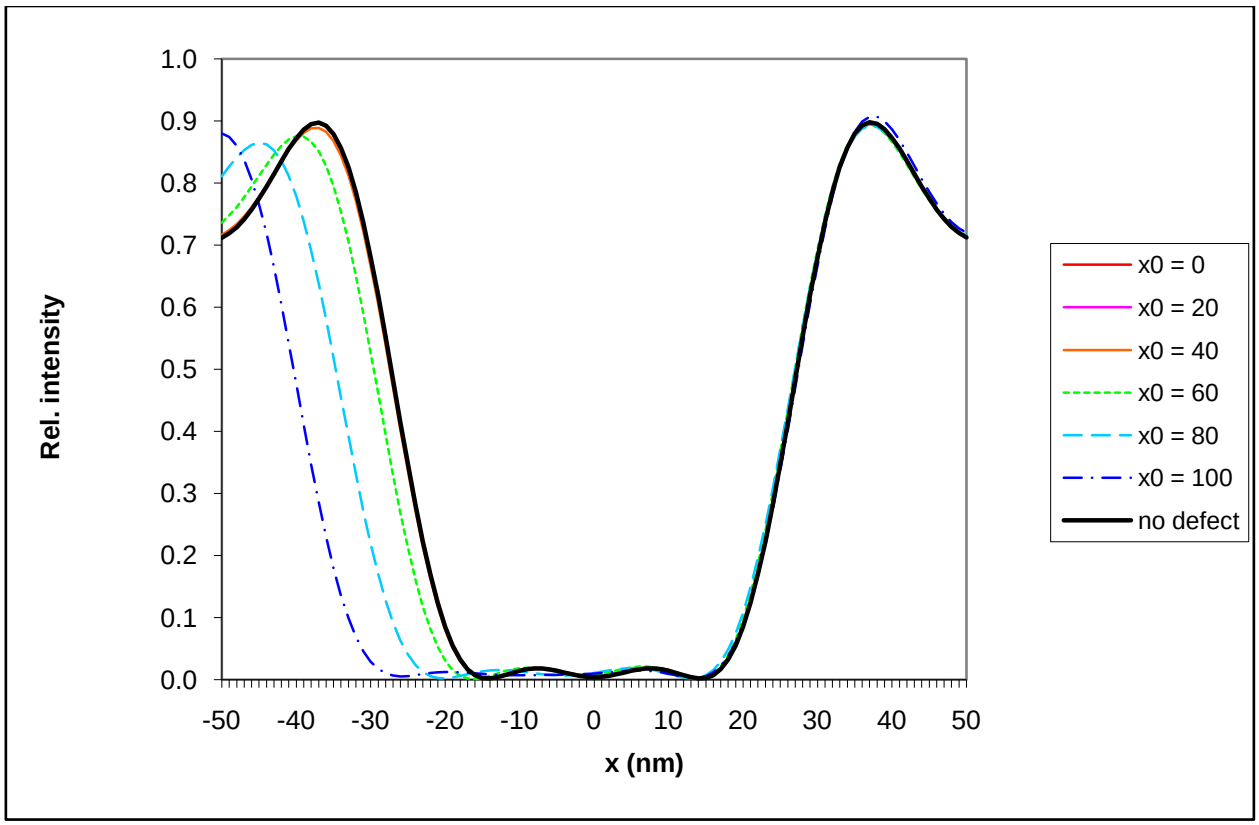

Figure 8: Simulated aerial images of a 40 nm absorber line (wafer coordinates) deteriorated by a defect (width = 30 nm, height = 26 nm on mask level) and the caused deformation of the complete multilayer system. The defect is lateral offset relative to the center of the absorber by a distance x0 (on mask level). The defect free case is shown as a reference (black solid line).

Next, we want to know what is going to be happen if we would planarize the multilayer system. To this end we pick the worst case of the previous simulation (x0 = 100 nm) and modify the multilayer system corresponding to figure 7 (RHS). This means that the top 40 layers are flattened and only the bottom 40 layers remain deformed. The simulated aerial images are plotted in figure 9. It is evident that the planarization clearly reduces the observed CD increase of figure 8. The aerial image for the partly planarized multilayer stack (dotted curve) almost coincides with the aerial image of the

defect free mask (red solid curve) and the CD change is much smaller compared to the unplanarized case (dashed curve). The reason for this is that the planarization supresses the thin film interferences of the deformed layer stack and let them only weakly contribute to the aerial image.

Finally, it should be said that the EUV litho simulations were based on a pure 2D model. A more realistic 2D modeling would require to include the conical diffraction case for out of plane illumination waves. Nevertheless, we think that the examples showed how powerfull the C-RCWA method could be for EUV modeling and also, of course, for the rigorous forward simulation of EUV masks for optical or EUV scatterometry. And here it is noteworthy to say that the EUV litho simulations of the complete 80 layer masks took only seconds on an older 2GHz Pentium 4 CPU (± diffraction orders for C-RCWA) with non-optimized code.

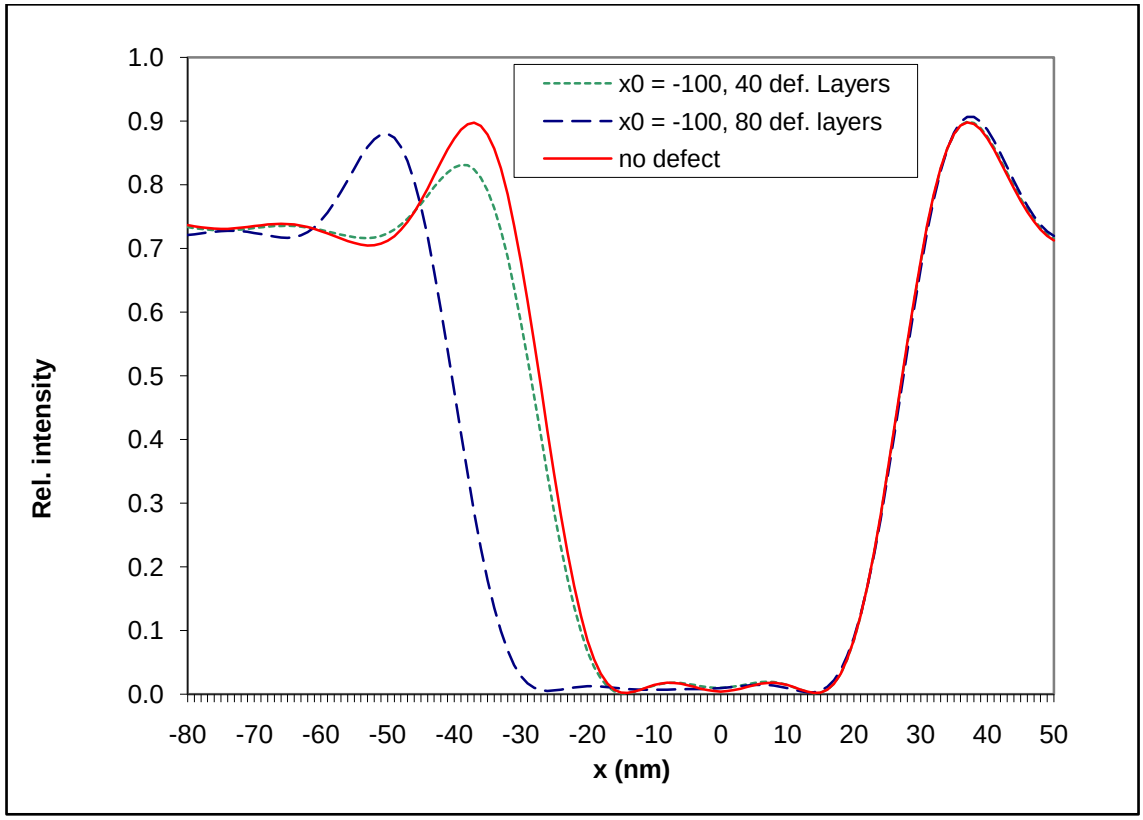

Figure 9: Simulated aerial images of a 40 nm absorber line (wafer coordinates) deteriorated by a defect (width = 30 nm, height = 26 nm on mask level) with different number of defect caused deformed layers. The aerial image of a defect free mask was plotted as a reference (solid curve).

5. Conclusions

A new method for diffraction computation was introduced which combines the RCWA and the Coordinate Transformation Method in a hybrid, S-matrix based algorithm. By means of a few simulation examples, it was shown that this method can overcome a lot of issues of the pure RCWA and the pure C-method. The application of this method can be particularly beneficial for the simulation of gratings with shallow prolife slopes and with many layers such as EUV masks. In some situations, the new method can enable a reasonable simulation at all. In many cases, it can help to reduce the computation costs dramatically and to improve the accuracy. Potential fields of application are in optical and EUV scatterometry as well as in optical and EUV lithography simulation. Further work has to be done to include conical diffraction and finally to address the 3D case, i.e. crossed gratings.

Acknowledgement

The author likes to thank Prof. G. Granet and Prof. J. Chandezon from Clermont-Ferrand University/ France for the beneficial and stimulating discussions about the C-method and the RCWA. Furthermore, the author is grateful to Dr. Andreas Erdmann from Fraunhofer Institute Erlangen/ Germany for providing some simulation input for the EUV example.

References

[1] Moharam, M.G., Pommet, D.A. and Grann, E.B., "Stable implementation of the rigorous coupled-wave analysis for surface-relief gratings: enhanced transmittance matrix approach," J. Opt. Soc. Am. A 12(5), 1077-1086 (1995).

[2] Li, L., "Multilayer modal method for diffraction gratings of arbitrary profile, depth and permittivity," J. Opt. Soc. Am. A 10(12), 2581-2591 (1993).

[3] Popov, E., Neviere, M., Gralak, B. and Tayeb,G., "Staircase approximation validity for arbitrary-shaped gratings," J. Opt. Soc. Am. A 19(1), 33-42 (2002).

[4] Chandezon, J., Maystre, D. and Raoult, G., ''A new theoretical method for diffraction gratings and its numerical application,'' J. Opt. (Paris) **11**, 235–241 (1980).

[5] Granet, G., Chandezon, J. and Plumey, J. P., "Reformulation of the coordinate transformation method through the concept of adaptive spatial resolution. Application to trapezoidal gratings," J. Opt. Soc. Am. A 18(9), 2102-2108 (2001).

[6] Granet, G., Plumey, J. P. and Chandezon, J., "Scattering by periodically corrugated dielectric layer with non-identical faces," Pure Appl. Opt. 4, 1-5 (1995).

[7] Li, L., Granet, G., Plumey, J. P. and Chandezon, J., "Some topics in extending the C method to multilayer gratings of different profiles," Pure Appl. Opt. 5, 141-156 (1996).

[8] Li, L., "Formulation and comparison of two recursive matrix algorithms for modeling layered diffraction gratings," J. Opt. Soc. Am. A 13(5), 1024-1035 (1996).

[9] Kleemann, B.H., Mitreiter, A. and Wyrowski, F., "Integral equation method with parametrization of grating profile - Theory and experiments," Journal of Modern Optics 43(7), 1323-1349 (1996).

[10] Elschner, J., Hinder, R. and Schmidt, G., "Finite element solution of conical diffraction problems," *Adv. Comput. Math.* **16,** 139-156 (2002).

[11] Evanschitzky, P. and Erdmann, A., "The Impact of EUV Mask Defects on Lithographic Process Performance," Proc. SPIE.5504, 111-119 (2004).